Spectrum of a lattice exciton in a transverse magnetic field: Emergence of full translational symmetry

Mona Berciu

Department of Physics and Astronomy, University of British Columbia, Vancouver, BC, Canada V6T 1Z1
and Quantum Matter Institute, University of British Columbia, Vancouver, BC, Canada V6T 1Z4

(Received 19 April 2013; revised manuscript received 10 June 2014; published 23 June 2014)

We show that even in the presence of a transverse magnetic field, the eigenstates of an exciton remain invariant to the full lattice translation group. This is expected if the exciton is viewed as a neutral quasiparticle, but not if one views it as a bound electron-hole pair. Single electron and hole wave functions are invariant only to the magnetic translation group, and their momenta are restricted to the magnetic Brillouin zone; the associated folding is the origin of their Hofstadter butterfly spectra. We find that such folding is not necessary for exciton eigenstates, which are characterized by momenta in the full Brillouin zone and thus have higher symmetry than the Hamiltonian. The magnetic field can have a significant effect on the shape of the exciton dispersion, however. While similar effects have been noted in continuous models, we find qualitatively different behavior for Frenkel excitons, whose origin we clarify. We also derive an analytical solution for the Hofstadter butterfly on a square lattice and analyze its dispersion in the full Brillouin zone.

DOI: 10.1103/PhysRevB.89.245128 PACS number(s): 71.35.Aa, 02.10.Ud, 71.35.Ji, 71.70.Di

I. INTRODUCTION

The spectrum of a charged particle moving on a two-dimensional (2D) lattice in a transverse magnetic field—the Hofstadter butterfly—has long been a fascinating topic in condensed matter physics [1,2]. The key result is that if the magnetic flux per unit cell Φ is a rational fraction of the elementary magnetic flux $\Phi_0 = \frac{h}{e}$, i.e., $\Phi = \frac{p}{q}\Phi_0$ where p,q are mutually prime integers, then the spectrum consists of q subbands. The reason is that due to the Peierls phases, the Hamiltonian is not invariant to all lattice translations, only to those in the magnetic translation group [3]. This group is associated with a magnetic unit cell q times larger than the original unit cell, so as to enclose an integer flux $p\Phi_0$. Consequently, the magnetic Brillouin zone (MBZ) is q times smaller than the full Brillouin zone (FBZ); this explains the q subbands of the butterfly as the result of folding the dispersion from the FBZ into the MBZ. We note that the Hofstadter butterfly has been recently observed in graphene [4] and there are suggestions for how to engineer effective "magnetic" fields in cold atom systems, which may provide another platform for investigating such Hamiltonians [5].

A charge neutral object has no corresponding Peierls phases, so a magnetic field should have no effect on its spectrum (hereafter, we ignore spin degrees of freedom). Naively, one would expect this to hold for an exciton, which is a bound electron-hole pair and thus neutral. However, the electron and the hole acquire Peierls phases and their individual wave functions are properly defined only in the MBZ. It is thus not *a priori* clear if the exciton eigenstates are defined in the FBZ, or the MBZ. Here, we show that the former holds true: Indeed, the exciton eigenstates continue to be characterized by momenta in the FBZ even in the presence of the magnetic field. Unlike in the naive picture, however, we do find that the exciton's dispersion may depend significantly on the magnetic field, since interference between the hole's and the electron's Peierls phases affects its motion.

In this work, the spectrum of a lattice exciton in a transverse magnetic field is investigated. Previous work focused on continuous models [6–9], where translations form a continuous group [7] and the momentum can have any value. By contrast, in lattice models the translation group is discrete and the question as to what is the proper Brillouin zone for the crystal momentum is meaningful. Also, while a dependence of the exciton's effective mass on the magnetic field was found in the continuous models as well, its origin is qualitatively different from what we find for lattice models, as discussed below. Moreover, the solution we provide here for the lattice problem is exact, whereas most of the work on continuous models is based on a projection into the lowest Landau level, i.e., assumes that the applied magnetic field is large enough that the gap opened between consecutive Landau levels is much larger than the typical electron-hole interaction energy. We make no such approximations here. In fact, since the Peierls phases are periodic functions of the magnetic flux and since they are the only way for the magnetic field to enter the model (see below), it is not even clear what a "large enough magnetic field" means in the lattice context.

The paper is organized as follows: Section II describes the specific 2D lattice models studied here and a possible experimental implementation. Section III shows that an analytical solution is possible for the propagator of a single charge-carrier hopping on a square lattice placed in a transverse magnetic field, both in the MBZ and the FBZ. Some of the relevant aspects of the Hofstadter butterfly spectrum in the unfolded Brillouin zone are then analyzed. Section IV generalizes this approach to calculate the electron+hole propagator, from which the exciton spectrum is extracted as the lowest-energy feature. The results are analyzed in Sec. V, while Sec. VI contains our conclusions.

II. MODEL

The Hamiltonian we investigate is

$$\mathcal{H} = -\sum_{\langle i,j\rangle} \left(t_{ij}^{(e)} c_i^\dagger c_j + t_{ij}^{(h)} h_i^\dagger h_j + \text{H.c.}\right) - \sum_{i,j} U_{ij} c_i^\dagger c_i h_j^\dagger h_j. \tag{1}$$

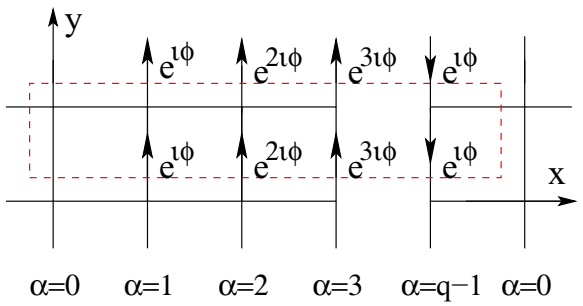

FIG. 1. (Color online) Magnetic unit cell consisting of q sites $\alpha = 0,\ldots,q-1$. The Peierls phases for electron (hole) hopping in (opposite to) the direction of the arrows equal $e^{i\alpha\phi}$.

The first term describes nearest-neighbor (NN) hopping on a 2D square lattice with $a = 1$, where the hopping integrals $t_{ij}^{(e/h)} = t_{e/h}\exp[\frac{\pm ie}{\hbar}\int_j^i \vec{A}(\vec{r})d\vec{r}]$ include the Peierls phases, and c_i and h_i are annihilation operators for an electron and hole at site i, respectively. We ignore the Zeeman coupling effects, so their spins are irrelevant. In the Landau gauge $\vec{A}(\vec{r}) = Bx\hat{e}_y$, the Peierls phases appear only for hopping along the y axis and are proportional to

$$\phi = 2\pi\frac{\Phi}{\Phi_0} = 2\pi\frac{p}{q}, \tag{2}$$

where p,q are mutually prime integers. The magnetic unit cell consisting of q adjacent sites and their Peierls phases are sketched in Fig. 1.

The second term is the electron-hole attraction. We consider both short-range (on-site) attraction $U_{ij} = U\delta_{ij}$, and long-range attraction $U_{ij} = U(i_x - j_x, i_y - j_y) = U/\sqrt{1+|i_x-j_x|^2+|i_y-j_y|^2}$. The geometry we envision is that of a bilayer with the electron and hole moving each in its own layer, like in biased coupled quantum wells with a modulation applied electrostatically through a lateral gate [10]. This gate could also be patterned with a 2D lattice, with a lattice constant large enough so that $\Phi \sim \Phi_0$ for reasonable values of B [11]. The short-range and long-range interactions correspond to having the lattice constant a large and small, respectively, compared to the distance between the two layers.

As we show below, both models give the same qualitative physics, although of course there are quantitative differences. This suggests that the answers to the specific questions we are interested in are universal, i.e., would be similar in other simulators of this problem. Given the recent progress [4], a biased graphene bilayer may offer another possible setup (on a honeycomb lattice), and many other implementations can be envisioned, including in the context of cold atoms trapped in optical lattices.

III. SINGLE CARRIER SPECTRUM

Before discussing the exciton spectrum, we briefly discuss the single carrier spectrum. This allows us not only to define the notation and explain how we implement the unfolding from the MBZ to the FBZ, but also to show that the Hofstadter spectrum can be calculated analytically for the square lattice.

There are q one-electron states with well-defined momentum in the MBZ, $\vec{k} \in (-\frac{\pi}{q},\frac{\pi}{q}]\times(-\pi,\pi]$, namely,

$$c_{\vec{k},\alpha}^\dagger = \sqrt{\frac{q}{N}}\sum_{i\in A_\alpha} e^{i\vec{k}\cdot\vec{R}_i}c_i^\dagger, \tag{3}$$

where $\alpha = 0,\ldots,q-1$ indexes distinct sites in the magnetic unit cell and A_α contains all lattice sites of type α. $N\to\infty$ is the total number of lattice sites.

Since Hamiltonian (1) is invariant to translations in the MBZ, $\langle 0|c_{\vec{k}'\beta}\hat{G}(\omega)c_{\vec{k}\alpha}^\dagger|0\rangle = \delta_{\vec{k}',\vec{k}}G_{\beta\alpha}(\vec{k},\omega)$. Here, $\hat{G}(\omega) = [\omega + i\eta - \mathcal{H}]^{-1}$ is the resolvent, $\eta\to 0_+$ is a small broadening, and we set $\hbar = 1$. The equations of motion for $G_{\beta\alpha}(\vec{k},\omega)$ are obtained from the matrix elements of the identity $\hat{G}(\omega)(\omega+i\eta-\mathcal{H}) = 1$, and read

$$\begin{aligned}(\omega+i\eta)&G_{\beta\alpha}(\vec{k},\omega)\\ &= \delta_{\alpha\beta} - 2t_e\cos(\alpha\phi - k_y)G_{\beta\alpha}(\vec{k},\omega)\\ &\quad - t_e[e^{-ik_x}G_{\beta,\alpha+1}(\vec{k},\omega) + e^{ik_x}G_{\beta,\alpha-1}(\vec{k},\omega)],\end{aligned} \tag{4}$$

where the cyclicity of α is implicitly assumed: if $\alpha = q-1$, then $\alpha+1 = 0$, etc. This system of q linear equations can be solved (see below) and the spectrum in the MBZ is extracted from the poles of any $G_{\beta\alpha}(\vec{k},\omega)$ propagator.

However, our goal is to calculate the Green's function $G(\vec{K},\omega) = \langle 0|c_{\vec{K}}\hat{G}(\omega)c_{\vec{K}}^\dagger|0\rangle$ defined in the original FBZ, for $\vec{K}\in(-\pi,\pi]\times(-\pi,\pi]$, where $c_{\vec{K}}^\dagger = 1/\sqrt{N}\sum_i e^{i\vec{K}\cdot\vec{R}_i}c_i^\dagger$ describes a free particle (for $B = 0$). This operator can be written in terms of $c_{\vec{k},\alpha}^\dagger$ where $\vec{k}\in$ MBZ is the value onto which $\vec{K}$ folds when going from the FBZ to the MBZ. For example, for $K_x > 0$ and an even γ so that $\vec{k} = \vec{K} - \gamma\frac{\pi}{q}\hat{x}$ lies in the MBZ, we have $c_{\vec{K}}^\dagger = 1/\sqrt{q}\sum_{\alpha=0}^{q-1}\exp(i\alpha\gamma\frac{\pi}{q})c_{\vec{k},\alpha}^\dagger$ and therefore $G(\vec{K},\omega) = 1/q\sum_{\alpha,\beta=0}^{q-1}e^{i(\alpha-\beta)\gamma(\pi/q)}G_{\beta\alpha}(\vec{k},\omega)$. Similar expressions (with somewhat different phase factors) are obtained for all other possible folding cases.

Let us introduce the generalized FBZ propagators:

$$G_n(\vec{K},\omega) = \frac{1}{q}\sum_{\alpha,\beta=0}^{q-1}e^{i(\alpha-\beta)\gamma(\pi/q)+i\alpha n\phi}G_{\beta\alpha}(\vec{k},\omega)$$

which are cyclic in $n = 0,\ldots,q-1$ and of which the $n = 0$ one is $G_0(\vec{K},\omega)\equiv G(\vec{K},\omega) = \langle 0|c_{\vec{K}}\hat{G}(\omega)c_{\vec{K}}^\dagger|0\rangle$. Using Eq. (4), we find that they satisfy the equations:

$$\begin{aligned}&[\omega+i\eta-\epsilon(K_x+n\phi)]G_n(\vec{K},\omega)\\ &\quad = \delta_{n,0} - t_e e^{-iK_y}G_{n+1}(\vec{K},\omega) - t_e e^{iK_y}G_{n-1}(\vec{K},\omega).\end{aligned} \tag{5}$$

This system of q linear equations can be solved analytically as follows. First, we treat the $n = 1,\ldots,q-1$ equations as a set of linear equations for the unknowns $G_1(\vec{K},\omega),\ldots,G_{q-1}(\vec{K},\omega)$. Inhomogeneous terms appear only in the $n = 1$ and $n = q-1$ equations and are proportional to $G_0\equiv G(\vec{K},\omega)$. It follows that we must have $G_n(\vec{K},\omega) = g_n(\vec{K},\omega)G(\vec{K},\omega)$ for all n. To simplify notations, from now on we use $g_n\equiv g_n(\vec{K},\omega)$. The $n = 0$ equation then gives the

solution in the expected form:

$$G(\vec{K},\omega) = \frac{1}{\omega + i\eta - \epsilon(K_x) - \epsilon(K_y) - \Sigma(\vec{K},\omega)} \tag{6}$$

with the self-energy of the particle in the magnetic field:

$$\Sigma(\vec{K},\omega) = -te^{iK_y}(g_{q-1} - 1) - te^{-iK_y}(g_1 - 1). \tag{7}$$

To find g_1 and g_{q-1}, we split the inhomogeneous system of linear equations into two parts: $g_n = F_n + H_n$, where

$$\begin{aligned}
[\omega + i\eta - \epsilon(K_x)]F_1 &= -t_e e^{iK_y} - t_e e^{-iK_y} F_2, \\
[\omega + i\eta - \epsilon(K_x + n\phi)]F_n &= -t_e e^{iK_y} F_{n-1} \\
&\quad - t_e e^{-iK_y} F_{n+1}, \\
\{\omega + i\eta - \epsilon[K_x + (q-1)\phi]\}F_{q-1} &= -t_e e^{iK_y} F_{q-2}
\end{aligned}$$

with $n = 2,\ldots,q-2$ in the central equations, and a similar set for $H_n, n = 1,\ldots,q-1$, but now with the inhomogeneous terms in the equation for H_{q-1}.

These can now be solved easily. For the F's, starting from $n = q-1$ it is immediate to see that $F_n = A_n F_{n-1}$, where the coefficient A_n is a finite continued fraction. The $n = 1$ equation then allows us to find all variables in terms of these continued fractions. For the H's, we start from $n = 1$ and find $H_n = B_n H_{n+1}$, again with simple finite continued fractions for coefficients; now the $n = q-1$ equation allows one to find all unknowns.

We can write both solutions in a compact form as follows. We introduce the finite continued fractions:

$$M_n(K_x,\omega) = \frac{t}{\omega + i\eta - \epsilon(K_x + n\phi) - tM_{n-1}(K_x,\omega)}$$

with $M_0(K_x,\omega) = 0$. Then for any $n = 1,\ldots,q-1$, $F_n = A_1 A_2 \cdots A_n$ where $A_n = -e^{iK_y} M_{q-n}(-K_x,\omega)$, and $H_n = B_{q-1} B_{q-2} \cdots B_n$ with $B_n = -e^{-iK_y} M_n(K_x,\omega)$.

As a result, the self-energy is

$$\begin{aligned}
\Sigma(\vec{K},\omega)/t_e = {} & M_{q-1}(K_x,\omega) + M_{q-1}(-K_x,\omega) + 2\cos(K_y) \\
& + e^{iq(K_y+\pi)} \prod_{n=1}^{q-1} M_n(-K_x,\omega) \\
& + e^{-iq(K_y+\pi)} \prod_{n=1}^{q-1} M_n(K_x,\omega).
\end{aligned}$$

The presence of M_{q-1}, with their $q-1$ continued-fraction "floors," agrees with the expectation of $q-1$ additional poles for $G(\vec{K},\omega)$ (q subbands in the spectrum). Note that $\Sigma(K_x,K_y,\omega)|_B = \Sigma(-K_x,K_y,\omega)|_{-B}$, $\Sigma(\vec{K},\omega) = \Sigma(-\vec{K},\omega)$, etc. However, there is no symmetry to 90° rotations, $\Sigma(K_x,K_y,\omega) \neq \Sigma(K_y,-K_x,\omega)$. The reason for this becomes clear if we plot the spectral weights in the BZ.

Before analyzing these spectra, we point out that the FBZ propagators are not diagonal in momentum, i.e., there are momenta $\vec{K} \neq \vec{K}'$ for which $\langle 0|c_{\vec{K}'} \hat{G}(\omega) c^\dagger_{\vec{K}}|0\rangle \neq 0$. This occurs, for instance, for any $\vec{K},\vec{K}'$ with $K_x > 0$, $K'_x < 0$ which map onto the same $\vec{k}$ value, and can be seen from the fact that the resulting set of linear equations [analogs of Eq. (5)] continue to have a nonzero inhomogeneous part although now it is not in the $n = 0$ equation, but in one with a finite n value. Physically, this shows that the FBZ is *not* the true Brillouin zone, as expected since the full lattice translations group is not the proper symmetry group of the Hamiltonian.

Plots of the single charge-carrier spectral weight $A(\vec{K},\omega) = -\frac{1}{\pi}\mathrm{Im}\, G(\vec{K},\omega)$ and of the density of states (DOS) $\rho(\omega) = \frac{1}{N}\sum_{\vec{K}} A(\vec{K},\omega)$ are shown in Fig. 2 for $\Phi = \frac{1}{q}\Phi_0$ with $2 \leqslant q \leqslant 5$. Since the spectral weight is very small in some regions of the FBZ, we superimposed solid (blue) lines which show the location of all the poles (i.e., the location of all eigenenergies). As expected, we see the q subbands. For even q, the two central subbands cross at a few Dirac points in the BZ, explaining the absence of a gap between them in the DOS.

The first two panels show the dispersion from $X_1 = (-\pi,0) \to \Gamma = (0,0) \to X_2 = (\pi,0)$. Not surprisingly, we see the q periodicity consistent with the folded MBZ used in the calculation. However, precisely the same periodicity appears on all other cuts in the BZ. For example, the subband energies on the $\Gamma \to X_2$ line are identical to those on the $\Gamma \to X_3 = (0,\pi)$ line, even though the MBZ was not folded along the y axis. This is correct: The spectrum cannot depend on the gauge used (which determined the folding of the MBZ), and must have the symmetry to 90° rotations of the underlying problem. What is sensitive to the gauge are the wave functions and thus the quasiparticle weights—indeed, these are different along otherwise equivalent lines. For example, along Γ-X_2 the weight shifts steadily from the lowest to the highest subband, whereas along Γ-X_3 most of the weight is in the lowest subband. Note that the sum rule $\int_{-\infty}^{\infty} d\omega\, A(\vec{K},\omega) = 1$ is obeyed at all $\vec{K}$.

In addition to the q periodicity for any cut in the BZ, we also see the reason for the existence of van Hove singularities in the DOS: these are due to the appearance of saddle points in the dispersion (e.g., the X points for $q = 3$). The evolution with increasing q (decreasing B) also becomes clear: The additional subbands are pushed to the top/bottom of the spectrum and become flatter. The expected dispersionless Landau levels spaced by the cyclotron frequency are indeed recovered as $B \to 0$.

This solution also allows us to understand the changes in the spectral weight for small variations of B. In Fig. 3 we show what happens to $A(\vec{K},\omega)$ when the flux is changed from $\Phi/\Phi_0 = 1/3$ to 10/31 and 100/301. The rough pattern remains the same, in particular three main subbands with $q = 3$ periodicity are seen in all cases. Of course, for the larger q there are, in fact, q rather flat subbands with their proper q periodicity. These are still visible in the $p/q = 10/31$ case, especially in the central "subband" where one can see pieces of the 11 true subbands that contribute to it. The top/bottom "subbands" have contributions from ten true subbands each, but their spacing is less than the broadening η and they merge into a broad feature in most places. This is certainly the case for $p/q = 100/301$ at all energies.

The weights in $A(\vec{K},\omega)$ also have similar patterns in all cases. For example, along $X_2 \to \Gamma$ the maximum weight moves from the upper to the lower subband, while along $\Gamma \to X_3$ the maximum is always in the lowest band. The flatness of the true subbands explains the lack of apparent dispersion along $\Gamma \to X_3$ for the $q = 31,301$ cases. This also

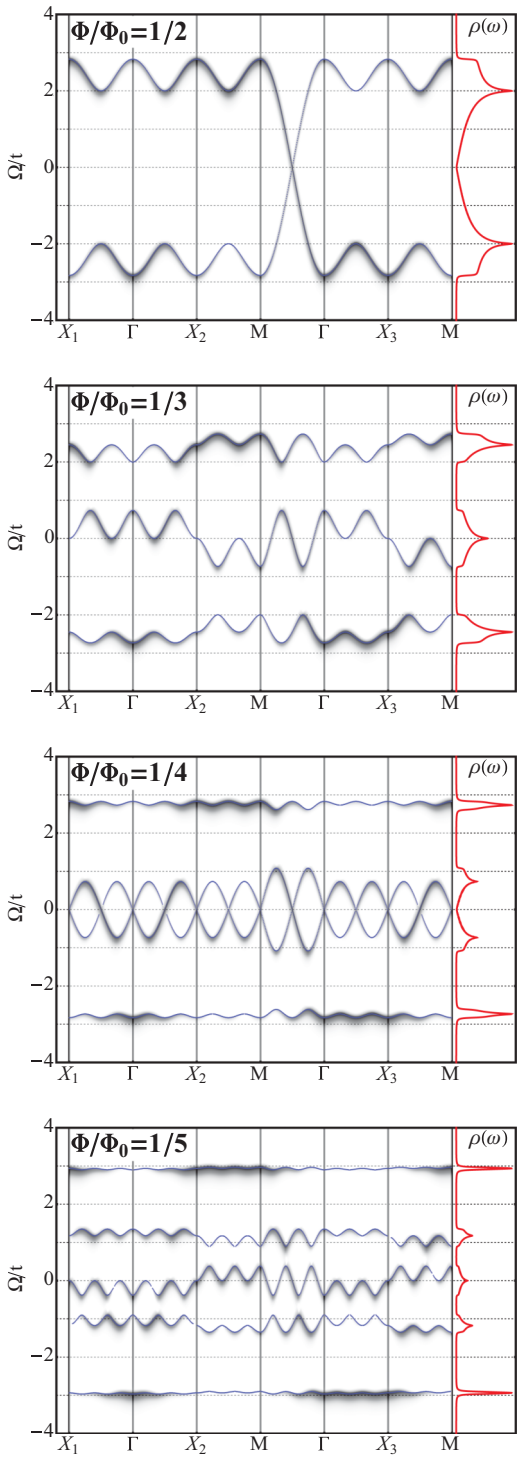

FIG. 2. (Color online) Electron spectra for $\Phi = \frac{1}{q}\Phi_0$ with $2 \leqslant q \leqslant 5$, along cuts between high-symmetry points $\Gamma = (0,0)$, $X_1 = (-\pi,0)$, $X_2 = (\pi,0)$, $X_3 = (0,\pi)$, and $M = (\pi,\pi)$ in the FBZ. Solid (blue) lines show the eigenstates, overlayed over the spectral weight (contour plots with broadening $\eta = 0.05$). The rightmost panels show the total DOS $\rho(\omega)$ versus ω.

illustrates the danger of attributing meaning to the contour plots of $A(\vec{K},\omega)$. For $q = 31,301$, the spectrum is very similar at all $\vec{K}$ points, and consists of many flat true subbands bunched into the three visible 'subbands. The apparent dispersion in

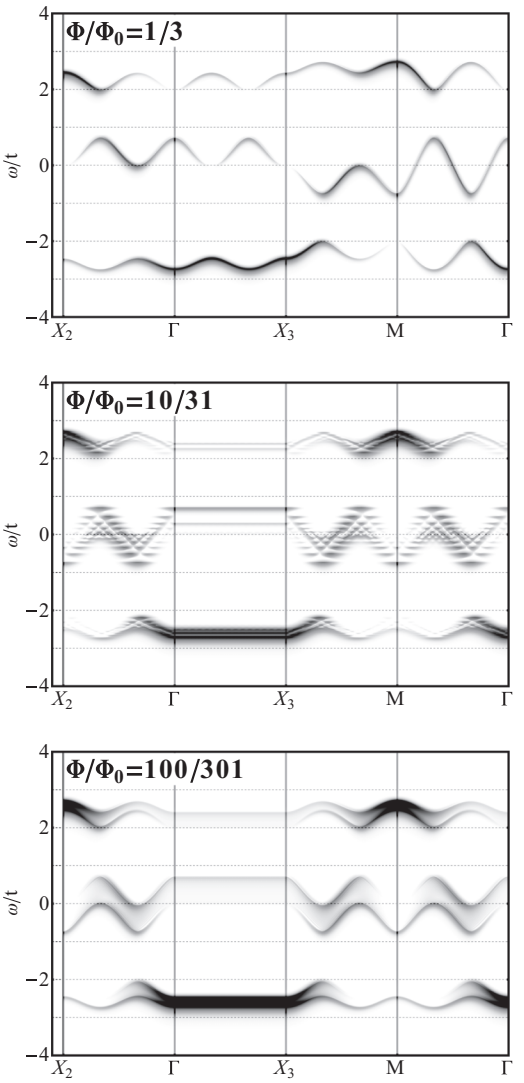

FIG. 3. Single charge-carrier spectral weight $A(\vec{K},\omega)$ for $\Phi = \frac{p}{q}\Phi_0$ with $p/q = 1/3,\ 10/31$, and $100/301$, along cuts between high-symmetry points in the FBZ, for $t = 1,\ \eta = 0.05$.

$A(\vec{K},\omega)$ is simply because of the shift of the spectral weight between these many subbands, not because their location changes with $\vec{K}$, as is normally the case. A different gauge will select a different looking "dispersion", which will mock the corresponding $q = 3$ pattern. In any event, these results confirm that even gauge dependent quantities vary smoothly with small changes in the flux, as expected on physical grounds. Our analytical solution can be used to easily study many other issues, but we stop here.

IV. ELECTRON+HOLE PROPAGATORS IN THE FBZ

We now follow similar steps to calculate the FBZ Green's functions for electron+hole states, to find

$$\mathcal{G}(\vec{K},\omega) = \langle 0|e_{\vec{K}}\hat{G}(\omega)e^{\dagger}_{\vec{K}}|0\rangle,$$

where $e^{\dagger}_{\vec{K}} = 1/\sqrt{N}\sum_i e^{i\vec{K}\cdot\vec{R}_i}h^{\dagger}_i c^{\dagger}_i$ is defined in the FBZ. Note that other propagators are also obtained from this method (see

below) but we focus on this particular one because it has the largest spectral weight on the bound excitonic states of interest to us. We again start with the MBZ electron+hole propagators

$$\mathcal{G}_{\beta\alpha}(\vec{k},n,m,\omega) = \langle 0|e_{\vec{k},0,0,\beta}\hat{G}(\omega)e^{\dagger}_{\vec{k},n,m,\alpha}|0\rangle$$

with $e^{\dagger}_{\vec{k},n,m,\alpha} = \sqrt{q/N}\sum_{i\in A_\alpha} e^{i\vec{k}\cdot\vec{R}_i}h^{\dagger}_i c^{\dagger}_{i+n\hat{x}+m\hat{y}}$ describing a state of momentum $\vec{k}\in$ MBZ with the electron at $n\hat{x}+m\hat{y}$ away from the hole, the latter being on sublattice α. Taking matrix elements of the identity $\hat{G}(\omega)[\omega+i\eta-\mathcal{H}]=1$, we now find

$$\begin{aligned}
&[\omega+i\eta+U(n,m)]\mathcal{G}_{\beta\alpha}(\vec{k},n,m,\omega)\\
&\quad=\delta_{\beta\alpha}\delta_{n,0}\delta_{m,0}-(t_h e^{i\alpha\phi-ik_y}+t_e e^{i(\alpha+n_q)\phi})\\
&\qquad\times\mathcal{G}_{\beta\alpha}(\vec{k},n,m-1,\omega)-(t_h e^{-i\alpha\phi+ik_y}+t_e e^{-i(\alpha+n_q)\phi})\\
&\qquad\times\mathcal{G}_{\beta\alpha}(\vec{k},n,m+1,\omega)-(t_h e^{-ik_x}+t_e)\\
&\qquad\times\mathcal{G}_{\beta\alpha}(\vec{k},n-1,m,\omega)-(t_h e^{ik_x}+t_e)\\
&\qquad\times\mathcal{G}_{\beta\alpha}(\vec{k},n+1,m,\omega),
\end{aligned}$$

where $n_q = n \pmod q$ and $U(n,m)=U\delta_{n,0}\delta_{m,0}$ or $U_{n,m}=U/\sqrt{1+n^2+m^2}$ for short-range or long-range interactions, respectively. This is an infinite system of coupled linear equations, with an inhomogeneous term only in the equations for $\mathcal{G}_{\alpha\alpha}(\vec{k},0,0,\omega)$.

These equations can be solved as discussed below. However, since we are interested in the FBZ propagators, we use these equations to first generate equations of motion for the FBZ propagators, which we then solve. The mapping between FBZ and MBZ operators is done like for single carriers; for instance, for $K_x>0$ and even γ mapping $\vec{K}\to\vec{k}+\gamma\frac{\pi}{q}\vec{x}$, we have $e^{\dagger}_{\vec{K}}=\frac{1}{\sqrt{q}}\sum_{\alpha=0}^{q-1}e^{i\alpha\gamma(\pi/q)}e^{\dagger}_{\vec{k},0,0,\alpha}$, etc. Suppresing the $\vec{K},\omega$ indices to compactify the notation, let

$$g_{nm}(\vec{K},\omega)\equiv g_{n,m}=\frac{1}{q}\sum_{\alpha,\beta}e^{i(\alpha-\beta)(\gamma\pi/q)-im\alpha\phi}\mathcal{G}_{\beta\alpha}(\vec{k},n,m,\omega).$$

The propagator of primary interest to us is $\mathcal{G}(\vec{K},\omega)\equiv g_{0,0}$. The equations of motion for g_{nm} are generated from those for $\mathcal{G}_{\beta\alpha}$ listed above. They read as follows:

$$\begin{aligned}
&[\omega+i\eta+U(n,m)]g_{nm}\\
&\quad=\delta_{n,0}\delta_{m,0}-(t_h e^{-iK_y}+t_e e^{in_q\phi})g_{n,m-1}\\
&\qquad-(t_h e^{iK_y}+t_e e^{-in_q\phi})g_{n,m+1}-(t_h e^{-iK_x+im\phi}+t_e)g_{n-1,m}\\
&\qquad-(t_h e^{iK_x-im\phi}+t_e)g_{n+1,m}.
\end{aligned}$$

Even though this is an infinite system of coupled equations, an arbitrarily accurate solution can be obtained by truncating it at a sufficiently large Manhattan distance N_c, i.e., by assuming that all $g_{nm}\to 0$ if $|n|+|m|\geqslant N_c$. The cutoff N_c is increased until the results converge. For exciton (bound) states this cutoff can be quite small, $N_c\sim 10$, since in excitonic states it is exponentially unlikely to find a large distance between the electron and the hole. For higher-energy states in the continuum describing (unbound) scattering states of the electron and hole, the cutoff needs to be much larger since, in principle, the electron and the hole can be arbitrarily far apart. In practice, however, the broadening η defines a finite lifetime $\tau\sim 1/\eta$ which prevents the electron and hole from moving arbitrarily far apart. As a result, for results to converge N_c only needs to be larger than the typical distance traveled by carriers within this lifetime τ. The resulting finite linear and very sparse system of equations is solved numerically [12] and the FBZ spectrum is obtained from the poles of $\mathcal{G}(\vec{K},\omega)\equiv g_{00}(\vec{K},\omega)$. As mentioned above, this also gives us all other propagators g_{nm} with $|n|+|m|<N_c$, not just g_{00}.

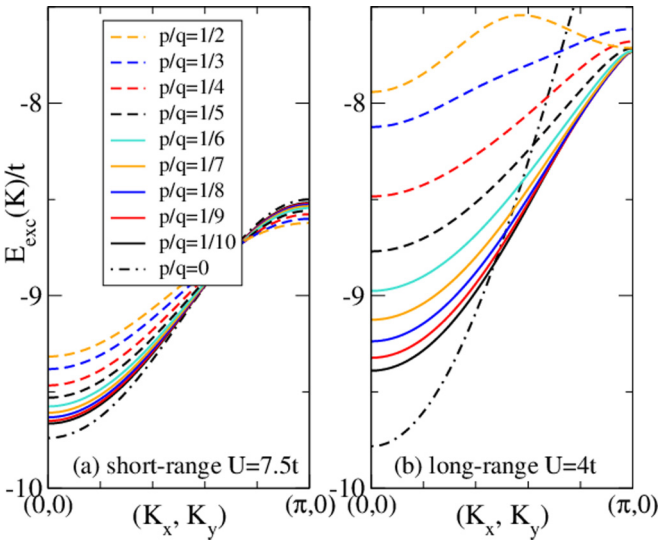

FIG. 4. (Color online) Exciton dispersion along the (0,0)-(π,0) cut in the FBZ, for several values of ϕ and $t_e=t_h=t$.

V. RESULTS

In Fig. 4 we plot the exciton dispersion $E_{\rm exc}(\vec{K})$ defined as the lowest-energy pole of the electron+hole propagator $\mathcal{G}(\vec{K},\omega)$ for a given $\vec{K}$, along the (0,0)-(π,0) cut in the FBZ, for several values of Φ. We show results for $\frac{p}{q}<0.5$ because the spectra are invariant to $\Phi\to\Phi+\Phi_0$ and $\Phi\to-\Phi$. Panel (a) is for short-range attraction with $U=7.5t$, while panel (b) is for long-range attraction with $U=4t$. These values were chosen so that the exciton binding energy at $B=0$ is similar.

The first observation is that there is no trace of the q periodicity apparent in the single particle dispersion. For any panel in Fig. 2 one can easily identify the true Brillouin zone (the MBZ) for the single charged particle from the fact that the dispersion must mirror its periodicity and therefore the slope of the dispersion must vanish at the Brillouin zone edges. Indeed, this occurs at π/q values. By contrast, the slope of the exciton dispersion is finite everywhere inside the FBZ, showing that this must be the true Brillouin zone for this neutral object. The curves have similar (though not identical) shapes irrespective of their Φ/Φ_0 ratio, showing no sign of any underlying MBZ-related periodicity. To put it another way, for these exciton dispersions choosing a larger unit cell and therefore a smaller Brillouin zone would result in a folded dispersion that would not have zero slope at the boundaries of this smaller Brillouin zone. This is similar to what would happen in the absence of the magnetic field for a single particle;

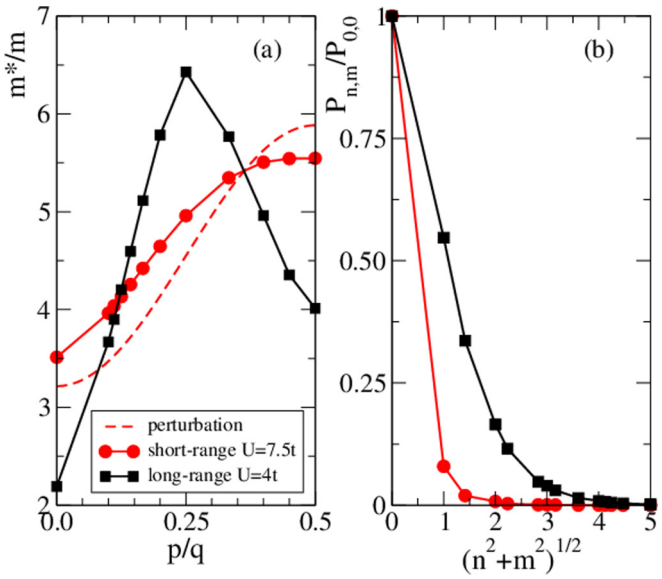

FIG. 5. (Color online) (a) Effective mass of the exciton vs $p/q = \phi/(2\pi)$, for the same parameters as in Fig. 4. (b) Corresponding probabilities $P_{n,m}$ to find a relative distance $n\hat{x} + m\hat{y}$ between the electron and the hole, in the $B = 0$ ground state of the exciton, normalized with respect to $P_{0,0}$.

of course one could choose a larger unit cell and therefore find the free-particle dispersion $\epsilon(\vec{K}) = -2t(\cos K_x + \cos K_y)$ folded in the appropriate number of subbands. None of those subbands has zero slope at the edges of the folded Brillouin zone, though, showing that the dispersion is not periodic within this small Brillouin zone and therefore that it is not the true (largest possible) Brillouin zone.

We find similar results (not shown) along all other cuts in the Brillouin zone and also for different ratios of t_e/t_h, so long as neither hopping vanishes. This confirms that these exciton eigenstates are indeed properly defined in the FBZ, in agreement with general expectations for neutral objects. The dispersions, however, do change with B, this being more apparent for the longer-range interaction. To quantify this change, we calculate the effective mass of the exciton from the curvature of its dispersion at $K = 0$. The results are shown in Fig. 5(a), in units of the mass m of a single particle with hopping t. The effective mass shows significant dependence of B.

To understand the reason for this dependence, we use perturbation theory to fourth order in $|t_e|$ and $|t_h|$ to calculate the exciton's dispersion in the case with short-range attraction. The zeroth-order solution is an immobile Frenkel exciton with the hole and electron at the same site, and energy $-U$. Standard calculations lead to

$$E_{\rm exc}(\vec{K}) = E_0 - 2t_1^*(\cos K_x + \cos K_y) - 4t_2^* \cos K_x \cos K_y - 2t_3^*[\cos(2K_x) + \cos(2K_y)] + \cdots,$$

i.e., the dispersion of a quasiparticle (the exciton) with up to third nearest neighbor hopping, which is indeed well defined within the FBZ irrespective of the applied magnetic field. The effective on-site energy and hopping integrals for the exciton

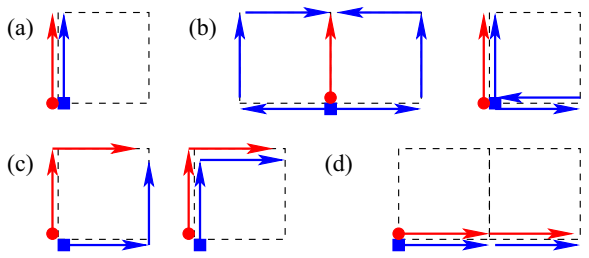

FIG. 6. (Color online) Examples of contributions to NN exciton hopping in (a) and (b), and to second and third NN exciton hopping in (c) and (d), respectively. In panels (b) and (c), the first example leads to Aharonov-Bohm interference and thus magnetic field dependence, while the second does not. The hole and electron are depicted with different symbols and their hopping is indicated by arrows of different colors.

are

$$E_0 = -U - \frac{4(t_e^2 + t_h^2)}{U} - \frac{8(t_e^4 + t_h^4)\cos\phi - 4(t_e^2 - t_h^2)^2}{U^3},$$

$$t_1^* = \frac{2t_e t_h}{U} + \frac{4t_e t_h(t_e^2 + t_h^2)}{U^3}(2\cos\phi - 1) + \cdots,$$

$$t_2^* = \frac{4t_e^2 t_h^2}{U^3}(3\cos\phi - 1) + \cdots,$$

$$t_3^* = -\frac{2t_e^2 t_h^2}{U^3} + \cdots.$$

Consider now the effective exciton hopping integrals. The only second-order term is $2t_e t_h/U$ in t_1^*, due to processes depicted in Fig. 6(a) where either the electron hops to a NN site and is then followed by the hole, or vice versa. They follow the same path so their Peierls phases cancel out and there is no ϕ dependence. In fourth order, however, t_1^* acquires dependence of ϕ through processes where, for example, the hole moves to a NN site by one hop, while the electron goes to the same site by three hops on the other sides of the plaquette [see Fig. 6(b)]. This leads to an overall phase of $\pm\phi$ for these contributions and thus to Aharonov-Bohm interference between them. Of course, there are also fourth-order contributions independent of ϕ, one of which is sketched in Fig. 6(b).

Fourth-order perturbation in hopping also generates effective second and third NN exciton hopping. The former contains a term dependent on (independent of) ϕ, describing contributions from processes where the electron and the hole move on the opposite (same) sides of a plaquette [see Fig. 6(c)]. The third NN hopping is independent of ϕ since no phase is acquired in fourth order [see Fig. 6(d)], although ϕ dependence appears in higher orders.

The ratio between the exciton effective mass and the mass of either charge carrier $m_{e/h} \sim (t_{e/h})^{-1}$ is

$$m^*/m_{e/h} = U/(2t_{h/e}) + \left[t_e^2 + 4t_e t_h + t_h^2 - 2(t_e^2 + 3t_e t_h + t_h^2)\cos(\phi)\right]/(Ut_{h/e}) + \cdots.$$

This is in reasonable agreement with the short-range result in Fig. 5(a) (see dashed line), although higher-order terms are required for good quantitative agreement at this still modest value $U = 7.5t$. Note that if either t_e or t_h vanish, then the

effective exciton mass becomes infinite as the exciton will be pinned near this immobile charge. Of course, in that case the question of a Brillouin zone again becomes nonsensical, as the immobile carrier breaks translational symmetry.

For the long-range potential, the dependence of m^* on ϕ is much stronger. This is expected given that in this case the exciton wave function is much more extended, as shown in Fig. 5(b) where we plot the probability $P_{n,m}$ to find the electron at a distance $n\hat{x} + m\hat{y}$ from the hole in the ground state at $B = 0$ (this quantity can be extracted from the residues associated with the exciton pole, of the various propagators g_{nm}). This exciton is more Wannier-like, with larger average distance between the electron and the hole, and therefore there are many more contributions to its hopping where the electron and hole trajectories enclose larger magnetic fluxes, resulting in additional Aharonov-Bohm interference. However, these enclosed fluxes depend only on the difference between the hole and the electron trajectories, and not on their original starting point. This is why all the q sites in the magnetic unit cell are identical starting points, as far as the exciton dynamics is concerned, and so the normal unit cell is a valid choice and the corresponding FBZ characterizes the dispersion.

VI. DISCUSSIONS

To summarize, we have produced exact results for 2D lattice models of excitons moving in transverse magnetic fields, where the attraction between the electron and hole is modeled both by short-range and long-range interactions. In all cases we find that the exciton dispersion retains the FBZ as its proper Brillouin zone, i.e., these bound states retain the full translational invariance of the original lattice, despite the presence of the Peierls phases which reduce the translational symmetry of the Hamiltonian to that associated with the MBZ.

While this agrees with general expectations for the dispersion of a neutral object, we also find a strong dependence of the dispersion on the value of the applied magnetic field, which contradicts the naive expectations. As we showed, this is due to constructive or destructive interference between the phases accumulated by the constituent parts of the exciton—the electron and the hole—as they move together through the lattice. Thus, the dependence must be a periodic function of the "quantum of phase" $\phi = 2\pi\Phi/\Phi_0$, since the phase accumulated on any trajectory is an integer multiple of this.

This suggests the interesting possibility that quantum oscillations in various transport and thermodynamic properties should arise in excitonic systems, despite the absence of a Fermi surface.

This periodic dependence on ϕ is qualitatively different from that found in continuous models, which is through the magnetic length $l = \sqrt{\hbar/eB}$ and is monotonic, not periodic; e.g., for the lowest-energy exciton (associated with the electron and hole occupying states in the lowest Landau level), one finds [8] that $m^* \sim \sqrt{B}$. This dependence has nothing to do with interference between trajectories, like for a lattice model; there is certainly no "quantum of phase" in a continuous model. Instead, it arises through the modulations of the magnitude of the effective Coulomb attraction, which is controlled by l since the magnetic length defines the typical "spread" of the electron and hole wave functions.

We also note that Aharonov-Bohm oscillations of excitons have been discussed in the context of particles constrained to move on a ring [13]. While the underlying idea of interference is the same, that problem is very different from the one we consider here. In particular, there is no sense in discussing what is the discrete translational symmetry group and associated Brillouin zone for a ring, just as there is none for continuous models.

One interesting question is whether this invariance of the exciton eigenstates to all lattice translations can be inferred from group-theoretical considerations, or is it an emergent property that only applies to the bound sector of electron+hole eigenstates. In favor of the former possibility is the fact that one can easily verify that these electron+hole propagators are diagonal in the FBZ, i.e., $\langle 0|e_{\vec{K}'}\hat{G}(\omega)e^{\dagger}_{\vec{K}}|0\rangle = \delta_{\vec{K}',\vec{K}}\mathcal{G}(\vec{K},\omega)$. This is to be contrasted with the single-electron or single-hole propagators, which have nonvanishing matrix elements between momenta $\vec{K}' \neq \vec{K}$, as mentioned before, and which clearly signal that for charged particles the FBZ is not a symmetry group. However, while the orthogonality is necessary for the higher symmetry to be valid, it is not clear that it is a sufficient condition, as well.

Indeed, counterarguments are easy to find. To begin with, there are electron+hole propagators obtained by sandwiching the resolvent not between the $e^{\dagger}_{\vec{K}}|0\rangle$ states, but between FBZ Bloch states where the hole and electron are at a finite separation. In that case, one can find nonvanishing results for $\vec{K}' \neq \vec{K}$. This is not such a surprise if one considers the continua of states that must appear above the exciton bound state and describe scattering states where the electron and hole are not bound to each other. The energies of these states are given by the convolution of the single-electron and single-hole spectra, and should mirror their symmetry.

Indeed, this is illustrated for $p = 1$, $q = 3$ in Fig. 7, where we plot the electron+hole spectral weight $\mathcal{A}(\vec{K},\omega) = -\frac{1}{\pi}\mathrm{Im}\,\mathcal{G}(\vec{K},\omega)$ for $U = 0$ at energies corresponding to the lowest-energy electron+hole continuum. Figure 2(c) shows that the lowest single particle subband lies at $-2.75 < \omega/t < -2$, and the convolution should double these values (we choose $t_e = t_h = t$). Indeed, Fig. 7 shows a continuum of states between these expected bounds. The band edges of this continuum clearly show the $\pi/3$ periodicity expected for this

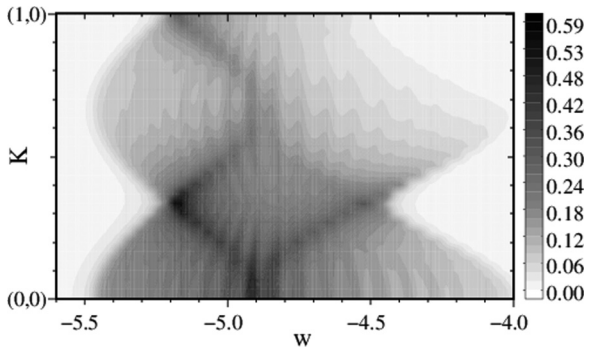

FIG. 7. Exciton spectral weight $\mathcal{A}(\vec{K},\omega)$ for energies in the lower electron+hole continuum, for $p = 1$, $q = 3$. Other paramerters are $t_e = t_h = 1$, $U = 0$, $\eta = 0.025$.

$q = 3$ situation (in the right upper corner the spectral weight vanishes so the true band-edge location is hard to see).

This continuum keeps its location for any value of U, since scattering states always appear at any energy in the convolution of the single-hole and single-electron spectra. What changes with U is that once the bound state appears, a lot of spectral weight is shifted into that state and the continuum is harder to "see." Its band edges and their MBZ periodicity remain the same, though. The remarkable fact is that the exciton dispersion shows no trace of this periodicity (see Fig. 4).

Since different parts of the spectrum exhibit different symmetries, it seems reasonable to conclude that the invariance to the full lattice translational group of the exciton eigenstates is an emergent property, valid only for the bound state. Indeed, only the bound state can be thought of as a charge neutral object (the exciton), for whom this higher symmetry is not unexpected.

These results provide an example of rather unusual eigenfunctions with *higher* symmetry than their Hamiltonian, and show that composite objects do not automatically inherit the translational properties of their constituent parts, but can have higher symmetry. In a very different context (and not based on an exact solution, like here) a similar situation was found in Ref. [14]. It would be interesting to understand to what extent this is a general occurrence, and what controls when it emerges.

ACKNOWLEDGMENT

This work was funded by NSERC and QMI.

[1] D. R. Hofstadter, Phys. Rev. B **14**, 2239 (1976).
[2] W. Y. Hsu and L. M. Falicov, Phys. Rev. B **13**, 1595 (1976); P. G. Harper, Proc. Phys. Soc., London, Sect. A **68**, 874 (1955); M. Ya. Azbel', Sov. Phys. JETP **19**, 634 (1964).
[3] J. Zak, Phys. Rev. **136**, A776 (1964).
[4] C. R. Dean, L. Wang, P. Maher, C. Forsythe, F. Ghahari, Y. Gao, J. Katoch, M. Ishigami, P. Moon, M. Koshino, T. Taniguchi, K. Watanabe, K. L. Shepard, J. Hone, and P. Kim, Nature (London) **497**, 598 (2013); L. A. Ponomarenko, R. V. Gorbachev, G. L. Yu, D. C. Elias, R. Jalil, A. A. Patel, A. Mishchenko, A. S. Mayorov, C. R. Woods, J. R. Wallbank, M. Mucha-Kruczynski, B. A. Piot, M. Potemski, I. V. Grigorieva, K. S. Novoselov, F. Guinea, V. I. Falko, and A. K. Geim, *ibid.* **497**, 594 (2013).
[5] D. H. Jaksch, Physics **5**, 60 (2012); J. Dalibard, F. Gerbier, G. Juzeliunas, and P. Ohberg, Rev. Mod. Phys. **83**, 1523 (2011).
[6] R. J. Elliott and R. Loudon, J. Phys. Chem. Solids **15**, 196 (1960).
[7] L. P. Gor'kov and I. E. Dzyaloshinskii, Sov. Phys. JETP **26**, 449 (1967).
[8] I. V. Lerner and Yu. E. Lozovik, Sov. Phys. JETP **51**, 588 (1980).
[9] S.-R. Eric Yang and L. J. Sham, Phys. Rev. Lett. **58**, 2598 (1987); Yu. A. Bychkov, T. Maniv, I. D. Vagner, and P. Wyder, *ibid.* **73**, 2911 (1994); M. Fritze, I. E. Perakis, A. Getter, W. Knox, K. W. Goossen, J. E. Cunningham, and S. A. Jackson, *ibid.* **76**, 106 (1996).
[10] M. Remeika, J. C. Graves, A. T. Hammack, A. D. Meyertholen, M. M. Fogler, L. V. Butov, M. Hanson, and A. C. Gossard, Phys. Rev. Lett. **102**, 186803 (2009).
[11] S. Melinte, Mona Berciu, Chenggang Zhou, E. Tutuc, S. J. Papadakis, C. Harrison, E. P. De Poortere, Mingshaw Wu, P. M. Chaikin, M. Shayegan, R. N. Bhatt, and R. A. Register, Phys. Rev. Lett. **92**, 036802 (2004).
[12] M. Berciu, Phys. Rev. Lett. **107**, 246403 (2011); M. Berciu and A. M. Cook, Europhys. Lett. **92**, 40003 (2010).
[13] For example, see A. Chaplik, Sov. Phys. JETP **62**, 900 (1995); R. A. Römer and M. E. Raikh, Phys. Rev. B **62**, 7045 (2000); A. Srivastava, H. Htoon, V. I. Klimov, and J. Kono, Phys. Rev. Lett. **101**, 087402 (2008); J. Shaver, S. A. Crooker, J. A. Fagan, E. K. Hobbie, N. Ubrig, O. Portugall, V. Perebeinos, Ph. Avouris, and J. Kono, Phys. Rev. B **78**, 081402(R) (2008); A. M. Fischer, V. L. Campo, Jr., M. E. Portnoi, and R. A. Römer, Phys. Rev. Lett. **102**, 096405 (2009).
[14] M. Berciu and S. John, Phys. Rev. B **61**, 16454 (2000).